Enantioselective Protein Affinity Selection Mass Spectrometry (EAS-MS)

Xiaoyun Wang[1,#], Jianxian Sun[1,2,#], Shabbir Ahmad[2,#], Diwen Yang[3], Fengling Li[2], U Hang Chan[2,4], Hong Zeng[2], Conrad V. Simoben [2], Scott Houliston[5], Aiping Dong[2], Albina Bolotokova[2], Elisa Gibson[2], Maria Kutera[2,5,6], Pegah Ghiabi[2], Ivan Kondratov[7,8,9], Tetiana Matviyuk[7,10], Alexander Chuprina[7], Danai Mavridi[11,12], Christopher Lenz[11,12], Andreas C. Joerger[11,12], Benjamin D. Brown[13], Richard B. Heath[13], Wyatt W. Yue[13], Lucy K. Robbie[14], Tyler S. Beyett[14], Susanne Müller[11,12], Stefan Knapp[11,12], Rachel Harding[2,4,15], Matthieu Schapira[2,4], Peter J. Brown[16], Vijayaratnam Santhakumar[2], Suzanne Ackloo[2], Cheryl H. Arrowsmith[2,5,6], Aled M. Edwards[2], Hui Peng[1,2,3*], Levon Halabelian[2,4*]

[1]Department of Chemistry, University of Toronto, Toronto, ON, Canada

[2]Structural Genomics Consortium, University of Toronto, Toronto, ON, Canada

[3]Department of Physical & Environmental Sciences, University of Toronto Scarborough, Toronto ON, Canada

[4]Department of Pharmacology and Toxicology, University of Toronto, Toronto, ON, Canada

[5]Princess Margaret Cancer Centre, University of Toronto, Toronto, ON, Canada

[6]Department of Medical Biophysics, University of Toronto, Toronto, Ontario, Canada

[7]Enamine Ltd., Winston Churchill Street 78, 02094 Kyiv, Ukraine

[8]Enamine Germany GmbH, Industriepark Hoechst, G837, 65926 Frankfurt am Main, Germany

[9]V. P. Kukhar Institute of Bioorganic Chemistry and Petrochemistry, National Academy of Sciences of Ukraine, Akademik Kukhar Street 1, 02094 Kyiv, Ukraine

[10]Department of Immunology and Infectious Diseases, Harvard T. H. Chan School of Public Health, Boston, MA, USA.

[11]Institute of Pharmaceutical Chemistry, Goethe University, Frankfurt am Main, Germany

[12]Structural Genomics Consortium, Goethe University, Frankfurt am Main, Germany.

[13]Biosciences Institute, Faculty of Medical Sciences, Newcastle University, Newcastle upon Tyne, UK.

[14] Emory University School of Medicine, Atlanta, GA, USA

[15]Leslie Dan Faculty of Pharmacy, University of Toronto, Toronto, ON, Canada

[16]Structural Genomics Consortium, Eshelman School of Pharmacy, University of North Carolina at Chapel Hill, Chapel Hill, NC 27599, USA

[#]These authors contribute equally to this work

*Corresponding authors:

Hui Peng: hui.peng@utoronto.ca; Structural Genomics Consortium, Department of Chemistry, University of Toronto

Levon Halabelian: l.halabelian@utoronto.ca; Tel: 416 946 3876; Structural Genomics Consortium, Department of Pharmacology and Toxicology, University of Toronto, Toronto

ABSTRACT

We report an enantioselective protein affinity selection mass spectrometry screening approach (EAS-MS) that enables the detection of weak binders, informs about selectivity, and generates orthogonal confirmation of binding. After method development with control proteins, we screened 31 human proteins against a designed library of 8,210 chiral compounds. 16 binders to 12 targets, including many proteins predicted to be "challenging to ligand", were discovered and confirmed in orthogonal assays. 7 binders to 6 targets bound in an enantioselective manner, with K_Ds ranging from 3 to 20 µM. Binders for four targets (DDB1, WDR91, WDR55, and HAT1) were selected for in-depth characterization using X-ray crystallography. In all four cases, the mechanism for enantioselective selectivity was readily explained. EAS-MS can be used to identify and characterize selective and weakly-binding ligands for novel protein targets with unprecedented throughput and sensitivity.

MAIN

Bioactive small molecules are invaluable reagents in basic research and applied fields such as biomedicine, agriculture and microbiology. The discovery of bioactive small molecules typically begins with screening of synthetic chemical or natural product libraries. Often, libraries of synthetic chemical or natural product libraries are screened in high-throughput or phenotypic screening[1-3] to identify compounds that alter biochemical or cellular functions. Alternatively, target-centric approaches can be employed, such as methods that measure binding to the target protein directly in vitro, including fragment-based lead discovery (FBLD)[4-6], DNA-encoded library (DEL) selection, or affinity selection mass spectrometry (ASMS)[7]. A significant challenge across all screening strategies is to develop orthogonal assays to distinguish true hits from false positives. Indeed, particularly when the initial hits bind weakly (> 10 µM K_D), this hit

verification process often demands more time and resources than the initial screen. As a result, it has proven impractical for the discovery of chemical ligands for large numbers of proteins.

Small molecules with a stereocenter may bind to their targets in an enantioselective way[10], which can be leveraged to identify potential steroselective protein binders when screening libreraied containing chiral compounds, as well as to develop negative controls for chemoproteomics studies and for experiments with chemical probes[11-13]. To exploit this phenomenon, we developed a scalable orthogonal screening strategy, termed "Enantioselective Protein Affinity Selection Mass Spectrometry (EAS-MS)", to both identify and characterize chemical ligands for previously unliganded proteins.

RESULTS

Design and benchmarking an Enantioselective Protein Affinity-Selection Mass Spectrometry (EAS-MS) platform

Method concept: The EAS-MS screening concept workflow (Fig. 1a) is a variation of previous methods used for bioactive natural product discovery[14-16], by including the orthogonal enantioselectivity evidence. First, pools of ~600 compounds from an 8,210 member screening library (Supplementary Table 1), comprising racemic mixtures of drug-like compounds at a concentration of 0.1 µM, are incubated with purified and quality-controlled polyhistidine-tagged proteins immobilized on magnetic nickel beads. At this concentration, all compounds are far below their solubility limit in aqueous solution. To embed a measure of selectivity in the screen, 8-12 different proteins are screened in parallel at a concentration of 1 µM in solution. This translates to an effective protein concentration of 100 µM on the beads. After washing the beads, compounds that remain bound to the proteins and the beads, which comprise a combination of real binders and nonspecific binders, are eluted in methanol. A small aliquot of each methanol

eluate is subject to liquid chromatography (LC) followed by high-resolution mass spectrometry in order to identify any compounds in the eluates, as well as to estimate their abundance relative to the eluates from other targets screened in parallel. Our concept is that some measure of binding specificity can be inferred by observing strong binding of a compound to one protein but not to the other proteins screened in parallel (8-12 proteins in each batch). For the compounds that appear to bind one target preferentially over the others, another aliquot from the same methanol eluate is analyzed by chiral chromatography, and the ratio of the two enantiomers in the protein eluate is assessed. If one of the two enantiomers is enriched in the protein eluate compared to their ratio in the screening library, then this provides orthogonal evidence for compound binding.

Proof of concept for EAS-MS with known enantioselective protein-ligand pairs. To pilot the EAS-MS concept, we selected four chiral compounds known to bind to their respective protein partners in an enantioselective manner. The first test case was lenalidomide, a chiral analogue of thalidomide that binds enantioselectively to the cereblon (CRBN) protein[17-19]. As shown in Fig. 1b, when screened against four proteins (CRBN, DCAF1, PRMT5, and USP21), lenalidomide was selectively enriched in the methanol eluate from CRBN beads; no significant enrichment was observed on beads containing any of the three other human proteins, which served as negative controls. The CRBN methanol eluate was then subjected to chiral chromatography. We recovered (*S*)-lenalidomide in the eluate from CRBN-containing beads at far greater quantities compared to its (*R*-) enantiomer, despite both being present in equal amounts in the input. Enantioselective binding was also observed for (*S*)-OICR0036766, (*S*)-LLY283, and (*R*)-BAY805, to their cognate protein targets, DCAF1[20], PRMT5[21], and USP21[22] (Fig. 1c, 1d, and 1e).

Racemate library design and characterization: With proof of concept in hand, we set out to apply the method to novel proteins, in screening mode. To this end, we assembled a diverse, drug-like screening library comprising 8,210 commercially available racemates, and developed chromatographic method(s) to resolve the enantiomers for as many of the racemates as was practical. These chemicals were selected by considering chemical diversity, drug-like properties and MS sensitivity (Fig. 1f and 1 g). To accomplish this, each of the 8,210 racemic mixtures was subject to chiral liquid chromatography under 8 different conditions (4 columns × 2 LC methods). In total, ~7,000 enantiomer pairs could be resolved under one of these conditions. The most effective chromatographic steps involved using IG and IA columns (Fig. 1h). Thus, for any of these 7,000 compounds, it is possible to compare the ratio of enantiomers in the screening library and the protein eluant, as described in the workflow outlined above (Fig 1a).

EAS-MS identifies low affinity binders. Rapid size-exclusion chromatography (SEC) is the most common approach used to resolve protein binders and non-binders in AS-MS library screening[7]. However, this method is known to be limited by the inability to detect weakly bound compounds, perhaps due to the challenges in retaining compounds with fast off-rates during chromatography. We explored whether the EAS-MS platform in which the protein is concentrated on beads and employs rapid wash steps, had the potential to enhance the sensitivity of AS-MS screens. Using 102 previously-characterized ligands across 8 proteins, we tested the sensitivity of EAS-MS. The EAS-MS platform successfully captured nearly all high-affinity ($K_D < 1$ μM) ligands, half of the moderate-affinity (1 μM $< K_D <$ 10 μM) ligands, and 20% of the low-affinity ($K_D > 10$ μM) ligands (Fig. 1i) without substantially increasing the false positive rate. In contrast, all moderate- and low-affinity ligands were lost by the SEC-coupled AS-MS approach. The apparent sensitivity of EAS-MS is a significant advantage for chemical ligand discovery, or to assess the

ligandability of a new protein, as binders can be discovered within a relatively small chemical library and by using lower amounts of protein.

Application of the EAS-MS platform to novel targets

With evidence of increased sensitivity and an ability to potentially provide orthogonal evidence for specificity using enantioselectivity, we set out to explore the application of the EAS-MS platform to new proteins. We selected 31 human proteins with diverse biological functions and with varying levels of known or predicted 'ligandability' (Fig. 2a) as assessed by their drug-like density (DLID) scores[23]. We purposely included several targets (*e.g.*, WDR91 and DCAF1) known to be 'ligandable' [20,24,25]. Among the 31 proteins, 3 were predicted to have high ligandability (DLID > 1), 11 of medium ligandability (0.5 < DLID < 1), and 16 low ligandability (DLID < 0.5) (Supplementary Fig. 1).

The 31 proteins were grouped in 4 batches of 8 proteins and screened against 14 pools of ~600 compounds. In total, 118 compounds (candidate binders) exhibited > 5-fold enrichment for one protein compared to the others screened in parallel, corresponding to an average hit rate of ~0.014% (Fig. 2b, and Supplementary Table 2). Candidate binders were detected for all three high ligandable targets, seven of the eleven targets with medium ligandability scores, and nine of the sixteen targets predicted to be the most challenging. Importantly, these hits were distributed across the entire chemical space of the EAS-MS library (Supplementary Fig. 2).

To confirm binding, we tested the binding of 101 candidate binders to each of the 18 targets using orthogonal methods. To this end, we used surface plasmon resonance spectroscopy (SPR), a technique that requires relatively small amounts of protein and when successful can provide quantitative orthogonal confirmation of binding. Ideally, SPR assay methods are developed using

a positive control binder, which we lacked for nearly all of the proteins. Accordingly, positive results by SPR can be interpreted, but negative results are inconclusive.

The binding of 16 hits to 12 targets was confirmed by SPR, ranging from 1-4 hits per target and with K_D values ranging from 2 to 87 μM (Fig. 2c and 2d; full list in Supplementary Table 2). Notably, 13 of the 16 SPR-confirmed hits exhibited low-affinity (K_D > 10 μM) (Fig. 1i). Interestingly, the degree of enrichment in the primary screen of the SPR-validated hits showed a strong correlation with the K_D values (Fig. 2e), demonstrating the potential application of the EAS-MS method for semi-quantitative read-outs.

As argued above, the 85 candidate binders that were unable to be confirmed using SPR are not necessarily false positives for three reasons. First, they might not be able to be detected because the assay for the protein target could not be optimized using a positive control compound. Second, they might also be *bone fide* binders with affinities beyond the sensitivity of SPR under the non-optimized solution conditions used. Third, the compounds might be insoluble at the concentrations required and conditions used for SPR (up to 0.2 mM of the compound) and might confound the read-outs[26]. The third possibility is a common issue when attempting to characterize weakly binding compounds by any biophysical method.

Enantioselective binding provides orthogonal evidence of compound binding

Our EAS-MS method, which creates an effective protein concentration of 100 μM on the beads, enables the screening of compounds at a concentration of 100 nM, far below their solubility limits. In support of solubility being a confounding issue for SPR orthogonal validation, we observed that SPR confirmation rates improved significantly for EAS-MS hits with higher fold enrichment values. For EAS-MS hits without enantioselectivity that were enriched > 5 fold, the SPR-confirmation rate was 12.2%; this increased to 22.2% for more potent hits with fold

enrichment values > 20 (Fig. 2f). For the more potent binders that were enantioselective enrichment, the SPR confirmation rate increased further to 50%. Even subject to the caveats of SPR, this trend clearly demonstrates the potential value of enantioselective enrichment in hit confirmation.

Among the 118 candidate binders identified in the screen of 31 proteins, clear enantioselective binding was detected for 32 binders to 14 targets (Fig. 2c). Of these targets, we were successful in developing an SPR assay for 6, and could calculate K_D values for 7 binders, with affinities ranging from 3-20 µM (Supplementary Figs. 4-8). There were 8 targets and 25 candidate binders for which we were unable to generate convincing binding data using either SPR under standard conditions or with other biophysical methods, such as differential scanning fluorimetry or ^{19}F-NMR. At this point, we cannot be certain if these 25 enantioselective candidate binders are false positives or are true positives that are challenging to assay.

In-depth characterization of enantioselective binding to 4 targets

Four targets – DDB1, WDR91, WDR55, and HAT1 - predicted to have 'medium' or 'low' ligandbility scores, as measured by their DLID scores (Fig. 2a, Supplementary Fig. 1), were selected for further analysis.

Damage-specific DNA-binding protein 1 (DDB1) is a multidomain protein involved in protein homeostasis[27]. We screened histidine-tagged DDB1 and 7 other proteins in parallel against the racemate library and identified a compound (XS381952) specifically enriched in the methanol eluate from DDB1 beads (Fig. 3a). When XS381952 in the DDB1-bead eluate was analyzed by chiral chromatography, one of the two enantiomers was clearly enriched compared with the ratio of the enantiomers in the starting library, providing compelling evidence of specific binding (Fig.

3b). To rigorously characterize the binding, we resolved and characterized the two enantiomers of XS381952 using preparative chiral chromatography and electronic circular dichroism (ECD) spectroscopy (Supplementary Fig. 3), and measured their binding to DDB1 using SPR. We found that (*S*)-XS381952 bound DDB1 with a K_D of 2 μM (Supplementary Fig. 4), significantly more potent than its (*R*)-counterpart (estimated K_D > 73 μM). To elucidate the mechanism of binding, we determined the crystal structure of (*S*)-XS381952 with DDB1 (Supplementary Table 3; Supplementary Fig. 9a), and found that (*S*)-XS381952 is sandwiched between two aromatic residues, W1047 and Y1114, via π-stacking interactions (Fig. 3c). The enantioselectivity was explained by the positioning of the ethoxyphenyl moiety linked to the chiral carbon, which adopted a nearly 90° angle from the compound backbone, orienting toward V1132 and stabilizing against the 1129-1140 *α*-helix of DDB1. The (*R*)-enantiomer would not be able to fit into the binding site due to steric hindrance.

WD40 repeat containing protein 91 (WDR91) is a 747-residue protein with a C-terminal WDR domain that plays a critical role in endosomal maturation[29]. After screening the WDR domain of WDR91 with racemate library, four compounds were enriched in WDR91-bead eluates compared with the other proteins screened in parallel. Two of these hits, XS838489 (Fig. 3d, 3e) and XS837729 (Supplementary Fig. 5), bound in an enantioselective manner. The remaining two hits, XS381295 and XS381186, did not show enantioselectivity in its binding. The binding of all four hits was characterized by SPR, and three hits displayed single digit micromolar K_D values (Supplementary Fig. 5), while the fourth hit, XS381186, displayed 29 μM K_D (Supplementary Fig. 5). To elucidate the binding mode of racemic XS838489, we co-crystallized it with the WDR domain of WDR91 (residues 392-747), revealing the (*R*)-enantiomer bound to WDR91 (Fig. 3f) (Supplementary Table 3; Supplementary Fig. 9b). This binding pocket lies between two

β-propellers and is surrounded by hydrophobic residues, including L465, L467, L477, and A459. The amide nitrogen linked to the chiral carbon forms a hydrogen bond with the backbone oxygen of T547, favoring the (*R*)-enantiomer for binding. The co-crystal structure of WDR91 with XS381295 showed it binding to the same side pocket also in an enantioselective manner (Supplementary Fig. 10), even though this was not apparent by EAS-MS. In the case of XS381295, its chlorophenyl ring fits into a hydrophobic pocket formed by the aliphatic side chains of L477, L465, L467, A459, as well as T547 and M550 (Supplementary Fig. 10). We suspect that the inability to detect enantioselective binding for XS381295 by chiral chromatography may be due to its rapid racemization.

WD40 repeat containing protein (WDR55) is a 383-residue WDR protein that adopts a seven-bladed β-propeller fold and functions as a nucleolar protein involved in ribosomal biogenesis[28]. Although WDR55 is predicted to be a challenging target according to its DLID score, racemic 'compound XS381774' was enriched (Fig. 3g, 3h), with a subsequently confirmed apparent K_D of 11 μM, as measured by SPR, and displayed enantioselectivity (Supplementary Fig. 6). The enantioselective binding of XS381774 was of some interest, because the enantiomers differed by the orientation of a single methyl group. The mechanism of enantioselective binding was revealed by co-crystallization of racemic XS381774 with WDR55 (Supplementary Table 3; Supplementary Fig. 9). The (*S*)-enantiomer of XS381774 preferentially co-crystallized in a hydrophobic side pocket of WDR55, and binding was mediated through hydrophobic interactions with the aliphatic side chains of residues I100, I108, V110, V122, L141, L135, and W153 (Fig. 3i). A methyl group which forms the chiral center points toward W153 and I108, enhancing hydrophobic interactions and that explained the enantioselective enrichment. To quantify the degree of selectivity, we separated and purified the individual enantiomers and

evaluated their binding affinities to WDR55 using SPR. The (*S*)-enantiomer of XS381774 exhibited at least 5-fold higher binding affinity compared to the (*R*)-enantiomer, with K_D values of 5 μM and > 25 μM, respectively (Supplementary Fig. 6).

Histone Acetyltransferase 1 (HAT1) is an enzyme that acetylates histone lysine residues, a modification associated with a transcriptionally active chromatin state[30]. Despite two decades of efforts in both academia and industry, there are few, if any, small molecule ligands for HAT1. In our EAS-MS screen, XS380871 was selectively enriched by HAT1 (Fig. 3j). Interestingly, XS380871 contains two chiral centers, and two of its four stereoisomers, were selectively enriched by HAT1 (Fig. 3k). The binding of XS380871 to HAT1, was confirmed by SPR (K_D = 12 μM) as well as ^{19}F NMR (Supplementary Fig. 7). To determine the molecular basis of binding, we incubated and co-crystallized the racemic mixture of XS380871 with HAT1 (Supplementary Table 3; Supplementary Fig. 9). The co-structure revealed that the compound binds at the acetyl-Coenzyme A (acetyl-CoA) binding site (Fig. 3l). The chiral carbon (*S*) linked to the nitrophenyl moiety exhibited an enantioselective binding mode, with the nitrophenol substituent forming hydrogen bonds with the backbone nitrogen of G253 (via its nitro group) and the backbone nitrogen of G249 (via its hydroxyl group). There would however be enough space elsewhere in the structure to accommodate the (*R*) enantiomer, albeit with potentially reduced affinity. In contrast, the fluorophenyl moiety at the second chiral carbon, bound to a hydrophobic subpocket lined by residues A275, V238, M241 and Y282; here the other enantiomer would be incompatible with binding due to severe steric clashes with the region around M241. This observation is consistent with the enantioselectivity data obtained from the EAS-MS analysis.

DISCUSSION

Despite the extensive efforts over the past decades[6], approximately 80% of all human proteins still lack chemical ligands[5,7,8]. The slow pace of chemical ligand discovery is largely due to the intrinsic limtations of the current chemical ligand discovery strategies. Here, we introduce the EAS-MS approach for high-throughput chemical ligand discovery: 1) The high sensitivity of the EAS-MS method in capturing weak-affinity hits ensures a high success rate, even with a relatively small chemical library (~8,000 compounds). This will reduce the time and financial cost for scalable screening. 2) Hit compounds may be able to be rapidly confirmed using orthogonal enantioselectivity information, bypassing time-consuming biophysical validations required for scalable and early-stage screening. The concept is that EAS-MS provides increased evidence of the specificity of compound binding not through use of an orthogonal assay with an orthogonal compound. Arguably, if a compound binds in an enantioselective manner in the screen at ~100 nM concentration, it may provide sufficient evidence of binding to obviate the need to test the compound at higher concentrations in an orthogonal biophysical assay. We envision that the EAS-MS approach will provide a convenient solution for scalable, proteome-wide chemical ligand discovery.

EAS-MS method may also be able to provide semi-quantitative information for identified hits. As shown in Supplementary Fig. 11, strong correlations were observed between the recovered MS signals of confirmed hits and their K_D values. This raises the possibility that the MS signals of EAS-MS hits can be used to generate large high-quality datasets that support artificial intelligence (AI)-based drug discovery.

Not all EAS-MS candidate binders could be confirmed using biophysical methods, such as SPR. Our limited data indicates this may be due to differences in their underlying biophysical principles: the SPR method can only detect hit compounds at concentrations above their K_D, which requires compounds to be soluble at high concentrations whereas EAS-MS is insensitive

to chemical concentrations. This discrepancy most apparent for weak EAS-MS hits, which may fail validation by SPR due to their low water solubility. Moving forward, we propose a general strategy of obtaining analogues of EAS-MS hits with greater predicted solubility as a strategy to facilitate biophysical validation.

REFERENCES

1 Moffat, J. G., Rudolph, J. & Bailey, D. Phenotypic screening in cancer drug discovery - past, present and future. *Nature reviews. Drug discovery* **13**, 588-602 (2014). https://doi.org:10.1038/nrd4366

2 Eder, J., Sedrani, R. & Wiesmann, C. The discovery of first-in-class drugs: origins and evolution. *Nature reviews. Drug discovery* **13**, 577-587 (2014). https://doi.org:10.1038/nrd4336

3 Macarron, R. *et al.* Impact of high-throughput screening in biomedical research. *Nature reviews. Drug discovery* **10**, 188-195 (2011). https://doi.org:10.1038/nrd3368

4 Parker, C. G. *et al.* Ligand and target discovery by fragment-based screening in human cells. *Cell* **168**, 527-541 e529 (2017). https://doi.org:10.1016/j.cell.2016.12.029

5 Abbasov, M. E. *et al.* A proteome-wide atlas of lysine-reactive chemistry. *Nature chemistry* **13**, 1081-1092 (2021). https://doi.org:10.1038/s41557-021-00765-4

6 Offensperger, F. *et al.* Large-scale chemoproteomics expedites ligand discovery and predicts ligand behavior in cells. *Science* **384**, eadk5864 (2024). https://doi.org:10.1126/science.adk5864

7 Prudent, R., Annis, D. A., Dandliker, P. J., Ortholand, J. Y. & Roche, D. Exploring new targets and chemical space with affinity selection-mass spectrometry. *Nature reviews. Chemistry* **5**, 62-71 (2021). https://doi.org:10.1038/s41570-020-00229-2

8 Durant, G., Boyles, F., Birchall, K. & Deane, C. M. The future of machine learning for small-molecule drug discovery will be driven by data. *Nature computational science* **4**, 735-743 (2024). https://doi.org:10.1038/s43588-024-00699-0

9 Wognum, C. *et al.* A call for an industry-led initiative to critically assess machine learning for real-world drug discovery. *Nature Machine Intelligence* **6**, 1120-1121 (2024).

10 Wang, Y. *et al.* Expedited mapping of the ligandable proteome using fully functionalized enantiomeric probe pairs. *Nature chemistry* **11**, 1113-1123 (2019). https://doi.org:10.1038/s41557-019-0351-5

11 Favalli, N. *et al.* Stereo- and regiodefined DNA-encoded chemical libraries enable efficient tumour-targeting applications. *Nature chemistry* **13**, 540-548 (2021). https://doi.org:10.1038/s41557-021-00660-y

12 Tao, Y. *et al.* Targeted protein degradation by electrophilic PROTACs that stereoselectively and site-specifically engage DCAF1. *Journal of the American Chemical Society* **144**, 18688-18699 (2022). https://doi.org:10.1021/jacs.2c08964

13 Ogasawara, D. *et al.* Chemical tools to expand the ligandable proteome: diversity-oriented synthesis-based photoreactive stereoprobes. *bioRxiv : the preprint server for biology* (2024). https://doi.org:10.1101/2024.02.27.582206

14 Yang, D. *et al.* Widespread formation of toxic nitrated bisphenols indoors by heterogeneous reactions with HONO. *Science advances* **8**, eabq7023 (2022). https://doi.org:10.1126/sciadv.abq7023

15 Liu, J. *et al.* Diindoles produced from commensal microbiota metabolites function as endogenous CAR/Nr1i3 ligands. *Nat Commun* **15**, 2563 (2024). https://doi.org:10.1038/s41467-024-46559-3

16 Liu, J. *et al.* The omega-3 hydroxy fatty acid 7(S)-HDHA is a high-affinity PPARα ligand that regulates brain neuronal morphology. *Science signaling* **15**, eabo1857 (2022). https://doi.org:10.1126/scisignal.abo1857

17 Ito, T. *et al.* Identification of a primary target of thalidomide teratogenicity. *Science* **327**, 1345-1350 (2010). https://doi.org:10.1126/science.1177319

18 Mori, T. *et al.* Structural basis of thalidomide enantiomer binding to cereblon. *Sci Rep* **8**, 1294 (2018). https://doi.org:10.1038/s41598-018-19202-7

19 Chamberlain, P. P. *et al.* Structure of the human Cereblon-DDB1-lenalidomide complex reveals basis for responsiveness to thalidomide analogs. *Nature structural & molecular biology* **21**, 803-809 (2014). https://doi.org:10.1038/nsmb.2874

20 Li, A. S. M. *et al.* Discovery of nanomolar DCAF1 small molecule ligands. *J Med Chem* **66**, 5041-5060 (2023). https://doi.org:10.1021/acs.jmedchem.2c02132

21 Bonday, Z. Q. *et al.* LLY-283, a potent and selective inhibitor of arginine methyltransferase 5, PRMT5, with antitumor activity. *ACS medicinal chemistry letters* **9**, 612-617 (2018). https://doi.org:10.1021/acsmedchemlett.8b00014

22 Göricke, F. *et al.* Discovery and characterization of BAY-805, a potent and selective inhibitor of ubiquitin-specific protease USP21. *J Med Chem* **66**, 3431-3447 (2023). https://doi.org:10.1021/acs.jmedchem.2c01933

23 Sheridan, R. P., Maiorov, V. N., Holloway, M. K., Cornell, W. D. & Gao, Y. D. Drug-like density: a method of quantifying the "bindability" of a protein target based on a very large set of pockets and drug-like ligands from the Protein Data Bank. *J Chem Inf Model* **50**, 2029-2040 (2010). https://doi.org:10.1021/ci100312t

24 Ahmad, S. *et al.* Discovery of a first-in-class small-molecule ligand for WDR91 using DNA-encoded chemical library selection followed by machine learning. *J Med Chem* **66**, 16051-16061 (2023). https://doi.org:10.1021/acs.jmedchem.3c01471

25 Ackloo, S. *et al.* A target class ligandability evaluation of WD40 repeat-containing proteins. *J Med Chem* (2024). https://doi.org:10.1021/acs.jmedchem.4c02010

26 Helmerhorst, E., Chandler, D. J., Nussio, M. & Mamotte, C. D. Real-time and label-free bio-sensing of molecular interactions by surface plasmon resonance: A laboratory medicine perspective. *The Clinical biochemist. Reviews* **33**, 161-173 (2012).

27 Jackson, S. & Xiong, Y. CRL4s: the CUL4-RING E3 ubiquitin ligases. *Trends in biochemical sciences* **34**, 562-570 (2009). https://doi.org:10.1016/j.tibs.2009.07.002

28 Iwanami, N. *et al.* WDR55 is a nucleolar modulator of ribosomal RNA synthesis, cell cycle progression, and teleost organ development. *PLoS genetics* **4**, e1000171 (2008). https://doi.org:10.1371/journal.pgen.1000171

29 Casanova, J. E. & Winckler, B. A new Rab7 effector controls phosphoinositide conversion in endosome maturation. *The Journal of cell biology* **216**, 2995-2997 (2017). https://doi.org:10.1083/jcb.201709034

30 Nagarajan, P. *et al.* Histone acetyl transferase 1 is essential for mammalian development, genome stability, and the processing of newly synthesized histones H3 and H4. *PLoS genetics* **9**, e1003518 (2013). https://doi.org:10.1371/journal.pgen.1003518

31 Hong, Y., Welch, C. J., Piras, P. & Tang, H. Enhanced structure-based prediction of chiral stationary phases for chromatographic enantioseparation from 3D molecular conformations. *Anal Chem* **96**, 2351-2359 (2024). https://doi.org:10.1021/acs.analchem.3c04028

32 Xu, H., Lin, J., Zhang, D. & Mo, F. Retention time prediction for chromatographic enantioseparation by quantile geometry-enhanced graph neural network. *Nat Commun* **14**, 3095 (2023). https://doi.org:10.1038/s41467-023-38853-3

METHODS

Reagents

Methanol (HPLC grade), ultrapure water (HPLC grade), acetonitrile (HPLC grade), DMSO, glycerol, and formic acid were purchased from Fisher Scientific (Ottawa, ON, CA). Ni-NTA magnetic agarose beads and Triton X-100 were obtained from Sigma-Aldrich (St. Louis, MO, USA). Tris base, sodium chloride (NaCl), Tris(2-Carboxyethyl)phosphine (TCEP) were sourced from BioShop Canada Inc. (Burlington, ON, CA). Imidazole was provided by Bio Basic Canada Inc. (Markham, ON, CA). The chemical library was purchased from Enamine US Inc. (Monmouth Jct., NJ, USA) and ChemDiv (San Diego, CA, USA). Stock solutions of the chemicals was prepared in DMSO and stored at -20 ^{o}C in the dark until use.

EAS-MS protein affinity selection experiments

The EAS-MS library of 8,210 chemicals was divided into 14 chemical pools by using a robotic system, with an average of ~600 chemicals in each pool. Each of the 14 chemical pools was incubated with purified recombinant His-tagged human proteins on 96-well plates, in the binding buffer (150 mM NaCl, 50 mM Tris-HCl, 0.1 mM TCEP, 0.5% glycerol, 0.01% Triton X-100, and pH 7.5). 5 µL of Ni-NTA magnetic beads was added to the binding buffer, adjusted to a final volume of 250 µL per sample. The final concentrations were set to 1 µM for the proteins and 100 nM for each chemical. All EAS-MS screenings were performed in triplicate. Incubation was carried out on a rotary mixer at 4 ^{o}C for 30 min. After incubation, the 96-well plate was placed on a magnetic plate to separate the beads, and the incubation buffer was removed. The beads were then washed twice with 100 µL of washing buffer 1 (150 mM NaCl, 50 mM Tris-HCl, 0.1 mM TCEP, 0.5% glycerol, 0.01% Triton X-100, 5 mM imidazole, and pH 7.5), followed by one wash with 100 µL of washing buffer 2 (150 mM NaCl, 50 mM Tris-HCl, 5 mM imidazole, and

pH 7.5). The beads and washing buffer 2 were transferred to a new plate. After removing the washing buffer 2, 120 μL of methanol was added to each well to denature proteins and release chemical ligands. The methanol extracts separated from magnetic beads were directly subjected to LC-MS analysis. In parallel, the extracts were also subjected to SDS-PAGE to confirm the presence of target proteins on the beads.

Identification of putative hits using LC-MS

The EAS-MS extracts were analyzed using an Orbitrap Exploris 240 mass spectrometer equipped with a Vanquish UHPLC system (Thermo Fisher Scientific, CA, USA). Chromatographic separation was conducted on an Accucore Vanquish C_{18} reverse-phase column (50 mm × 2.1 mm × 3 μm) at a flow rate of 0.3 mL/min. The injection volume was 1 μL. Ultrapure water with 0.1% formic acid (A) and methanol with 0.1% formic acid (B) were used as the two mobile phases. Gradient elution started with 5% B, increased to 80% at 1.5 min, then reached to 100% at 3 min, held for 1.1 min, and finally returned to 5% B over 1.5 min. The column temperature was maintained at 40 ^{o}C, and the sample compartment at 7 ^{o}C. Data acquisition was performed in full MS^1 scan mode (150-520 *m/z*) with a resolution of R = 60,000, in both positive and negative ionization modes. The detailed instrumental parameters of LC-MS system are provided in Table S4.

Chiral analysis of putative hits

1) Building the chiral separation database: the accurate prediction of suitable chiral separation conditions for resolving the enantiomers of a given compound remains a challenge[31,32]. To address this, we decided to establish the chiral separation database for the EAS-MS chemical

library, under eight conditions (4 columns × 2 LC gradient methods, see the details below). Each of the 14 chemical pools were individually injected under eight conditions to build the database.

2) Eight chiral separation conditions: four columns from DAICEL Chemical Industries, LTD. were employed: CHIRALPAK IA (250 × 4.6 mm), CHIRALPAK IBN (250 × 2.1 mm), CHIRALPAK IC (250 × 2.1 mm), and CHIRALPAK IG (250 × 2.1 mm). These columns were selected because they have been demonstrated to achieve sufficient separations for the biggest number of chiral compounds[31].

Two LC gradient methods were employed for each column. In **method 1**, acetonitrile with 0.1% formic acid (A) and methanol with 0.1% formic acid (B) were used as mobile phases. Gradient elution started at 40% B, held for 1 min, then increased to 80% at 3 min, reached 100% at 8 min, held for 1 min, followed by a return to 40% over 2 min, and held for another 1 min. The flow rate was set at 0.3 mL/min for columns IBN, IC, and IG, and at 1.0 mL/min for column IA.

In **method 2**, H_2O with 0.1% formic acid (A) and methanol with 0.1% formic acid (B) were used as mobile phases. Gradient elution began with 40% B, increased to 80% at 6 min, reached 100% at 18 min, held for 6 min, and then return to 40% over 6 min. The flow rate was 0.2 mL/min for columns IBN, IC, and IG, and 1.0 mL/min for column IA. The column temperature was maintained at 40 ^{o}C, and the sample compartment was kept at 7 ^{o}C. The injection volume was 1 µL.

3) Chiral detection of putative hits under optimal conditions: Once putative hits were detected from initial EAS-MS screening, the optimal separation condition for the hit compounds was selected by searching against the chiral separation database established in step 2) above. The same EAS-MS extracts were then analyzed under the optimal conditions. To exclude potential interferences, enantiomers were further confirmed by matching MS^2 spectra.

Automatic data processing

A total of 1,302 EAS-MS screening samples (31 proteins × 3 replicates × 14 pools = 1,302) were completed in the current study, leading to 145 GB of raw mass spectrometry data. We have established an automatic data processing workflow to detect EAS-MS hits (code is available on https://github.com/huiUofT/eCPIN).

1) Building the MS database for EAS-MS library: we first injected each of the 14 chemical pools to LC-MS analysis to build the database. In brief, raw mass spectrometry files were converted to the mzXML format. Peak features from each chemical pool were detected with the 'XCMS' R package at a mass tolerance of 2.5 ppm[29]. Only the peak features with peak intensity > 10^5, and 10 times higher abundances when compared to methanol were considered as library compounds and retained for subsequent data analysis. Isotopic peaks and adducts were excluded by matching chromatographic peaks and theoretical mass difference. The detected peak features were then matched to the EAS-MS library with a mass tolerance of 3 ppm. Potential inferences and misassigned compounds were further excluded via manual inspections. Then, a MS database of 8,210 EAS-MS library compounds were estalibshed, with *m/z*, retention time and SMILES information recorded.

2) Detecting compounds from EAS-MS features by matching to the MS database: to detect library compounds from the EAS-MS features, we matched each of the 8,210 EAS-MS compounds against each EAS-MS samples. A mass tolerance of 3 ppm, and a retention time matching window of 0.5 minutes were used. A final data matrix with 8,210 rows (corresponding to library compounds) and 24 columns (corresponding to EAS-MS samples from each batch) was created.

3) Detecting putative EAS-MS hits: to detect putative EAS-MS hits, we calculated the enrichment fold and *p* values of each library compound against each protein by using seven other proteins from the same batch as the control (equation 1).

Enrichment Fold = $A_{POI} \times N / \square A_i$ **(1)**

A_{POI} represents the peak intensity of the putative hit compound enriched by the protein of interest; N represents the number of background proteins from the same batch (N = 7); A_i represents the peak intensity of the same hit compound enriched by the ith protein from the same batch. Eventually, only the compounds with enrichment fold > 5, and *p* value < 0.05 were considered as putative hit compounds. Each putative hit was further manually inspected by matching to compound library, to exclude potential inteferences misassigned by the algorithms.

Quality Assurance and Quality Control (QA/QC) of EAS-MS

To assure the high-quality data for scalable EAS-MS screening, we conducted stringent QA/QC from both protein and chemical perspectives.

Protein QA/QC

To assure the selected proteins were properly folded and compatible with our EAS-MS workflow, we used SDS-PAGE to semi-quantitatively assess the recovery of each protein through our EAS-MS procedure. In brief, SDS-PAGE analysis was conducted for each protein before and after EAS-MS. The band intensity of each protein was compared, and those proteins with low recoveries were excluded for EAS-MS analysis. The SDS-PAGE results for all proteins are provided in Supplementary Fig. 12.

Chemical QA/QC

During LC-MS analysis, the EAS-MS chiral library compounds were injected every batch to ensure the retention time, *m/z*, and intensity are not shifting for database matching. All the chiral compounds were detected by the LC-MS system. A QC standard of small subset (~600

chemicals) was injected after every 12 samples to monitor instrument stability and LC (chiral) separations. The instrument response deviation for analytes in the QC standard remained below 10% throughout the analysis. A solvent blank was injected after every 12 samples to monitor and prevent carryover.

Proteins used for EAS-MS and SPR

Protein expression and purification summaries are detailed in Supplementary Table 5.

Crystallization and structure determination

Crystallization of EAS-MS hits with their respective targets are summarized in Supplementary Table 6.

Surface Plasmon Resonance

SPR hit confirmation and validations were performed using a Biacore 8K instrument at 20 °C. The biotinylated respective protein constructs were immobilized on the active flow cells of a Streptavidin-coated SA sensor chip after initial conditioning of both reference and active flow cells with 50 mM NaOH for 3 × 60 s with a flow rate of 10 μL/min. Each protein solution (30-150 μg/mL) was injected through the respective active flow cells for 60-660 s with a flow rate of 5 μL/min to obtain a desired protein immobilization level. Equilibration was performed after protein immobilization by flowing running buffer (50 mM HEPES, pH 7.5, 150 mM NaCl, 0.001% Tween 20, 0.2% PEG3350, 0.5 mM TCEP, and 3% DMSO) over the flow cells with a flow rate of 50 μL/min until a stable baseline was observed. Initial start-up cycles, blank cycles and wash (50% DMSO wash to flush the needles) steps were included in the SPR compound analysis methods. The compound injections were performed over the reference and active flow

cells using multi-cycle kinetics at a flow rate of 40 µL/min with a 55 s association time and a 120 s dissociation time for dose-response titration. The stock compound concentration series was performed in 100% DMSO with 2-3-fold serial dilution and prepared the samples using the running buffer by maintaining final DMSO concentration of 3% (v/v) across the tested concentration range. Initially, the compounds were titrated between 0-45 µM compound concentrations and later followed up between 0-15 µM, 0-30 µM, 0-45 µM, and 0-90 µM compound concentrations based on the affinity and solubility of the compounds. Solvent correction cycles were also included across each run to adjust high bulk responses from the solvent. Double referencing of the data was introduced by subtraction of the reference flow cell and the respective zero compound concentration cycles. Affinity fitting was performed by applying a 1:1 equilibrium binding model to the data using Biacore Intelligent analysis tool provided with the Biacore Insight Evaluation software. The final figures were prepared using GraphPad Prism.

^{19}F NMR studies

The binding of XS380871 to HAT1 was confirmed using ^{19}F NMR by looking for the broadening and/or shifting of its ^{19}F resonance upon the addition of HAT1. Spectra of the compound were acquired on a Bruker Avance III spectrometer operating at 600 MHz, equipped with a QCI probe at 293K, and collected at 20 µM, with and without the presence of HAT1 (~34 µM, buffered in 50 mM Tris 7.0, 200 mM NaCl, 4 mM DTT). TFA (100 µM) was added as an internal reference. 1k transients were acquired over a sweep width of 150 ppm; an exponential window function (LB = 5 Hz) was applied prior to Fourier transformation.

Statistics

All statistical analyses were conducted using GraphPad PRISM (GraphPad Software, Inc., La Jolla, CA). Data are presented as mean ± standard deviation. Statistical significance was determined using Student's *t*-test, with a significance threshold of $p < 0.05$.

DATA AVAILABILITY

Atomic coordinates and structure factors for all crystal structures have been deposited in the Protein Data bank under the accession codes: 9EJO, 9EJP, 9EJQ, 9EKP, 9MJG.

ACKNOWLEDGEMENTS

We would like to thank the advice and discussions on method development from Dafydd Owen (Pfizer), Judith Guenther (Bayer), Scott Johnson (Bristol Myers Squib), Oliver Kraemer (Boehringer Ingelheim), Julian Schmid (Merck), Juncai Meng (Janssen), Lawrence Szewczuk (Janssen), Xidong Feng (Pfizer), Wenyi Hua (Pfizer), Anja Giese (Bayer), Matteo Aldeghi (Bayer), Nidhi Arora (Takeda), James Kiefer (Genentech), Ingo Hartung (Merck), and Matthew Troutman (Pfizer). The Structural Genomics Consortium is a registered charity (no. 1097737) that receives funds from Bayer AG, Boehringer Ingelheim, Bristol Myers Squibb, Genentech, EU/EFPIA/OICR/McGill/KTH/Diamond Innovative Medicines Initiative 2 Joint Undertaking [EUbOPEN grant 875510], Janssen, Pfizer, and Takeda. Research was supported by a Natural Science and Engineering Research Council of Canada (NSERC) Discovery Grant, Ontario Early Researcher Award, and the National Institute of Health (NIH) (U54AG065187). The authors acknowledge the support of instrumentation grants from the Canada Foundation for Innovation, the Ontario Research Fund, and an NSERC Research Tools and Instrument Grant. A.C.J, S.M., and S.K. are also grateful for support by the German Cancer Aid grant TACTIC. TSB acknowledges startup funding provided by the Emory University School of Medicine and the

Winship Cancer Institute. AME holds the Temerty Nexus Chair of Health Technology and Innovation at the University of Toronto.

AUTHOR CONTRIBUTIONS

XW, JS, DY, AB, SA, PJB, VS, LH, HP, AME: EAS-MS method development

JS, XW: EAS-MS screening

HZ, PG, EG, MK, LKR, DM, CL: Protein production and QC

ShA, MK, FL: SPR, DSF confirmation

SH: F-NMR characterization

HZ, UHC, AD: X-ray crystallography

MS, CVS: Druggability assessment

SA, VS, PJB: Project management

WWY, RH, TSB, SM, ACJ, SK, LH, HP, AME, CHA: Supervision, review and editing

XW, JS, LH, HP: Writing, reviewing and editing with input from all

COMPETING INTERESTS

The authors declare no competing interests.

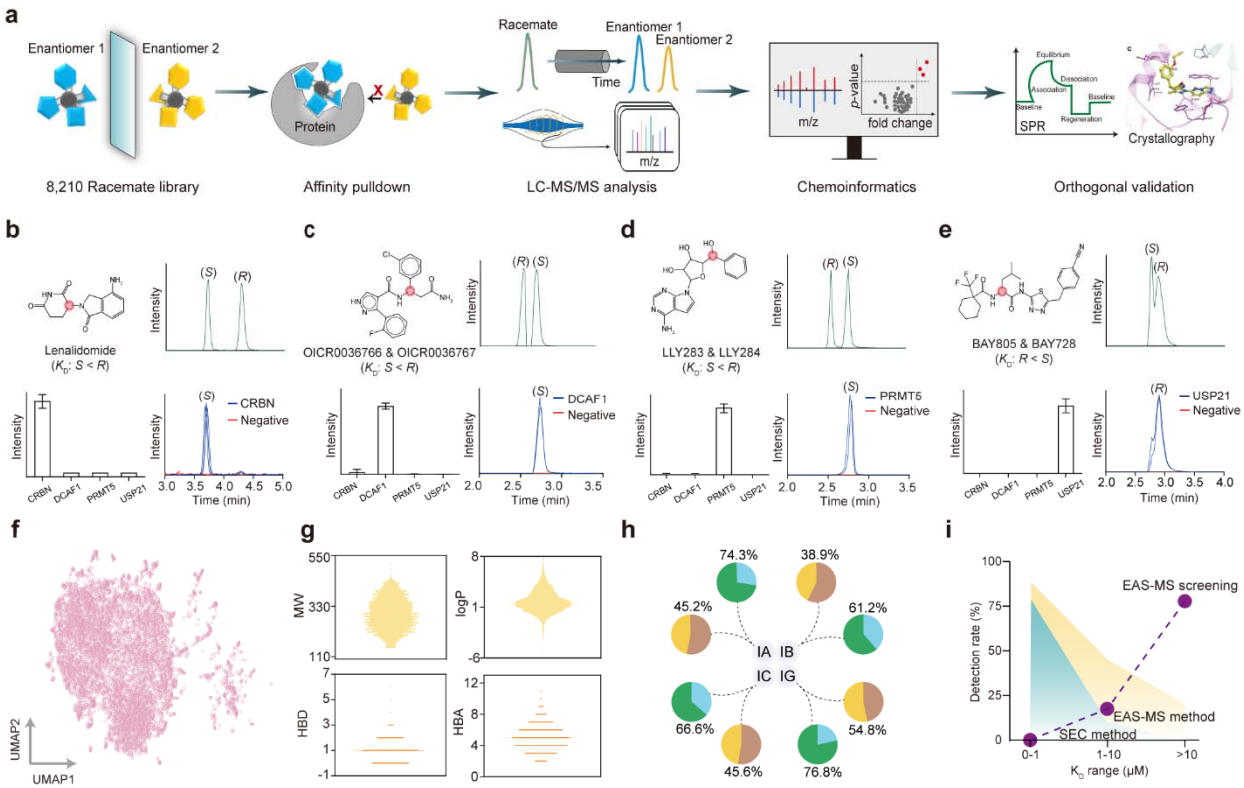

Fig. 1 | Development of the EAS-MS platform for scalable protein ligandability discovery. (**a**) Schematic representation of the EAS-MS screening workflow. (**b-e**) Benchmarking the EAS-MS platform using four positive control ligands binding to CRBN, DCAF1, PRMT5, and USP21, respectively. (**f**) Chemical space of the EAS-MS library. A two-dimensional uniform manifold approximation and projection (UMAP) visualization of SMILES descriptor. (**g**) Molecular properties of the EAS-MS chemical library: molecular weight (MW), LogP, hydrogen bond acceptors (HBA) and donors (HBD). **(h)** Chiral separation of the EAS-MS library using four chiral columns (IA, IB, IC, and IG), and two mobile phases (acetonitrile/methanol, yellow; water/methanol, green). **(i)** Detection rate of 102 ligands against 8 proteins by SEC and EAS-MS methods, respectively. Purple dots represent the K_D distribution of chemical ligands discovered by our own EAS-MS screening.

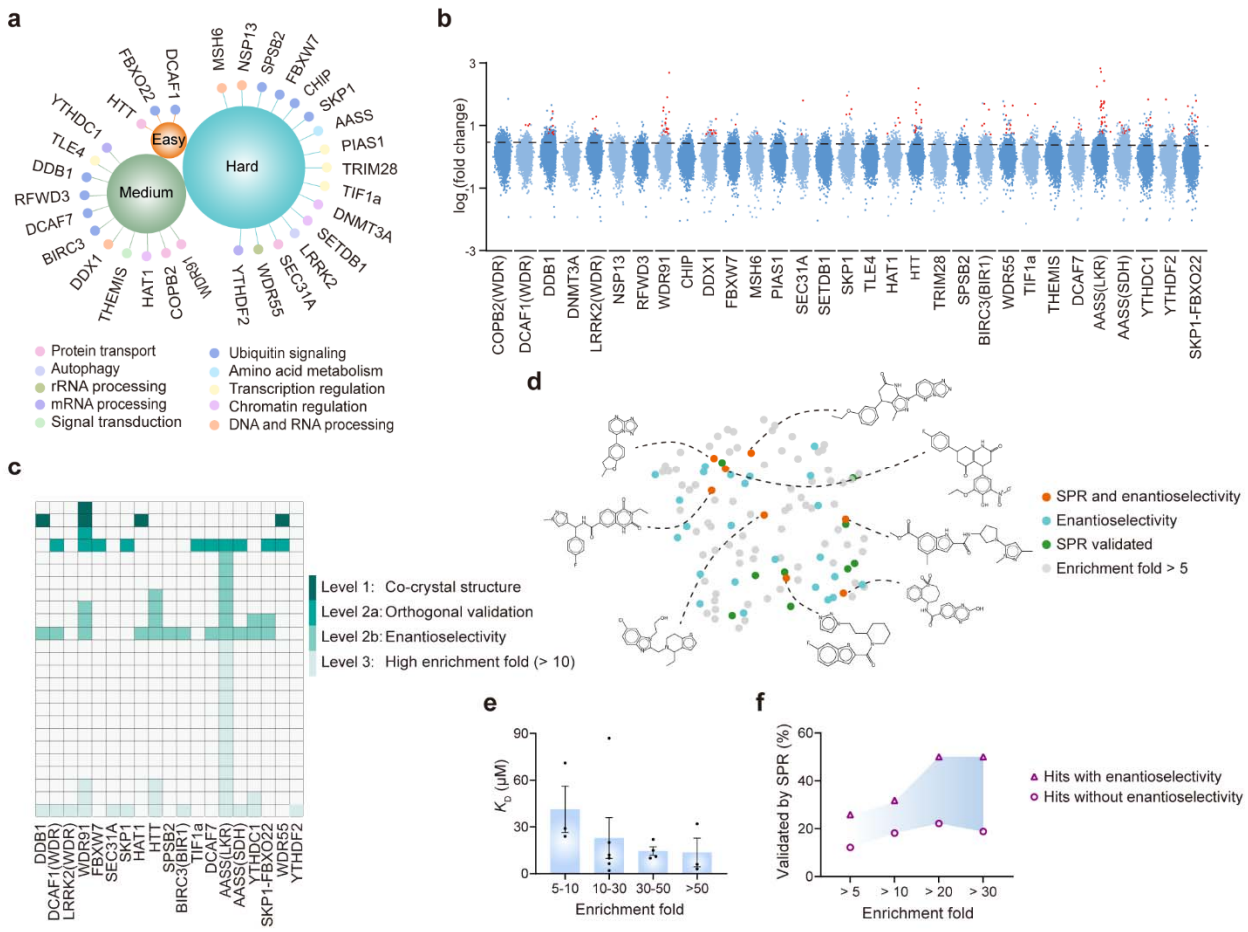

Fig. 2 | Scalable chemical ligand profiling across 31 diverse proteins. (**a**) Overview of the 31 screened proteins. 'High': drug-like density (DLID) > 1, 'Medium': 0.5 < DLID < 1, 'Low': DLID < 0.5. (**b**) Scatter plot of detected compounds interacting with all proteins. Dots above the line represent hits with enrichment fold > 5. Red dots indicate hits with enrichment fold > 5 and *p*-value < 0.05. (**c**) Confidence levels of all identified hits. (**d**) UMAP visualization of the chemical space for hits with enrichment fold > 5, based on SMILES descriptors. (**e**) Correlation between K_D and fold change. (**f**) SPR validation rate of hits across different enrichment fold ranges.

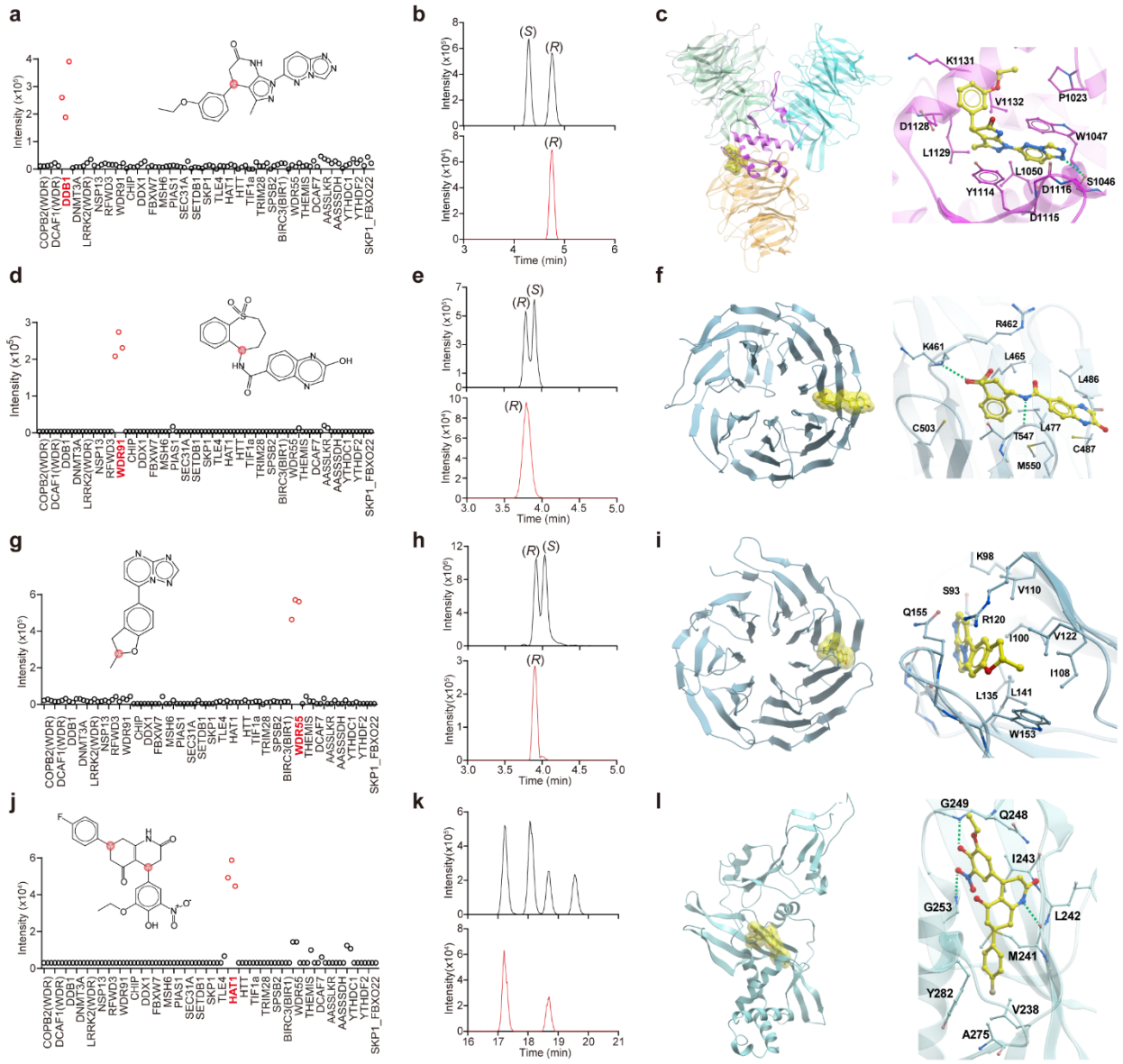

Fig. 3 | Identification of enantioselective hits for DDB1, WDR91, WDR55, and HAT1. (**a**) Scatter plot showing XS381952 pulled down by DDB1. (**b**) Chiral chromatogram of the XS381952 enantiomers. (**c**) Co-crystal structure of DDB1 with XS381952. Hydrogen bond between the protein and the ligand is shown as green dashed line (**d**) Scatter plot showing XS838489 pulled down by WDR91. (**e**) Chiral chromatogram of the XS838489 enantiomers. (**f**) Co-crystal structure of WDR91 with XS838489. Hydrogen bonds between the protein and the ligand are shown as green dashed lines (**g**) Scatter plot showing XS381774 pulled down by WDR55. (**h**) Chiral chromatogram of the XS381774 enantiomers. (**i**) Co-crystal structure of

WDR55 with XS381774. (**j**) Scatter plot showing XS380871 pulled down by HAT1. (**k**) Chiral chromatogram of the XS380871 enantiomers. (**l**) Co-crystal structure of HAT1 with XS380871. Hydrogen bonds between the protein and the ligand are shown as green dashed lines.

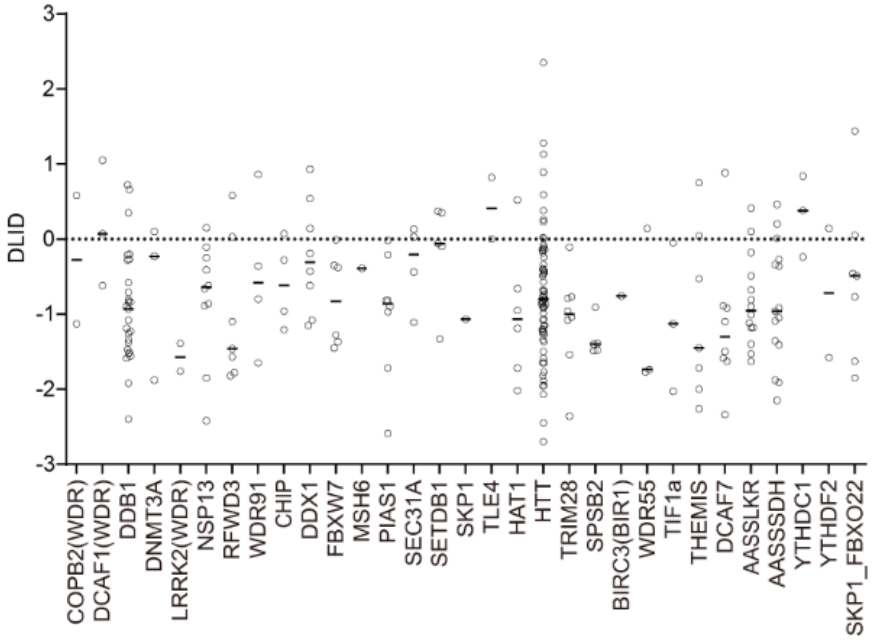

Supplementary Fig. 1 | Predicted ligandability of 31 selected proteins. Drug-like density (DLID) of each protein was predicted. The dots from each protein represents the predicted DLID score for each pocket in that protein. To define the ligandability of proteins, we used the maximal DLID score for the pocket from each protein. For instance, the maximal DLID score for HTT is 2.35 for the top drug-like pockets compared to other pockets, due to its large molecular size and surface. Proteins with low, medium and high ligandability were defined, as having maximal DLID scores < 0.5, 0.5-1, and > 1, respectively.

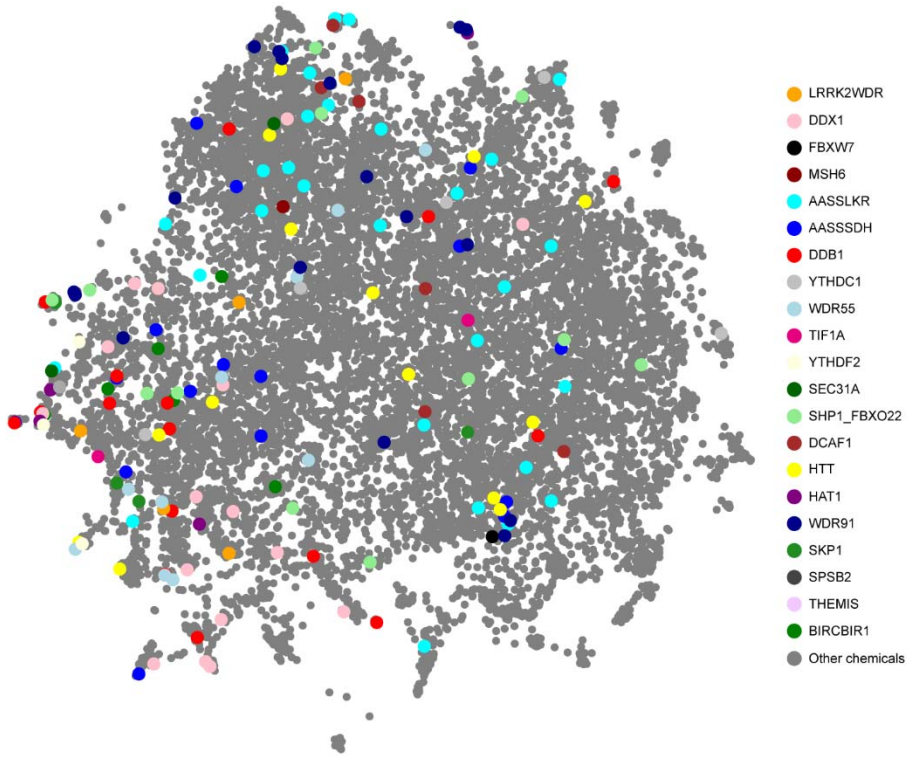

Supplementary Fig. 2 | Distribution of EAS-MS hits across the chemical space. UMAP visualization based on SMILES descriptor highlights the chemical distribution of identified hits.

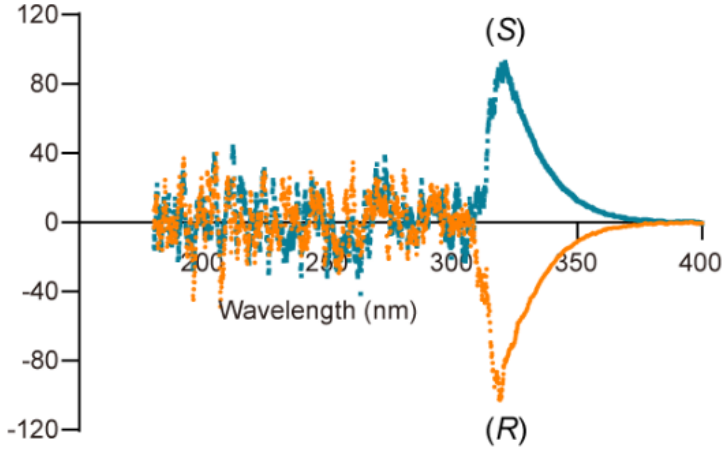

Supplementary Fig. 3 | ECD analysis of two enantiomers of XS381952 binding to DDB1. The two enantiomers were purified through the CHIRALPAK IA column.

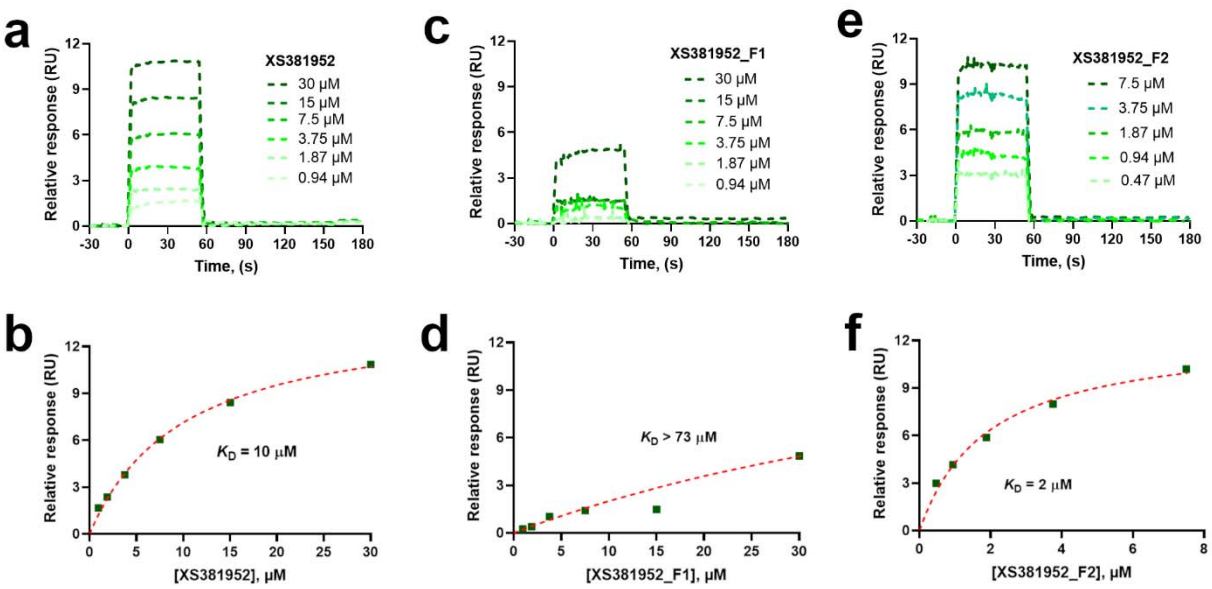

Supplementary Fig. 4 | Representative SPR sensorgrams (**a**, **c**, **e**) and the response vs concentration plots (**b**, **d**, **f**) for the DDB1 specific hit XS381952 (**a**, **b**) and its enantiomers XS381952_F1 (**c**, **d**) and XS381952_F2 (**e**, **f**) after separation, fraction 1 (100% pure) and fraction 2 (85% pure), respectively. The response at equilibrium for each concentration were plotted against the compound concentration and affinity fitted by applying 1:1 equilibrium binding model to extract the K_D of the interaction. The compounds were tested in duplicates. Data from one replicate is shown here for clarity.

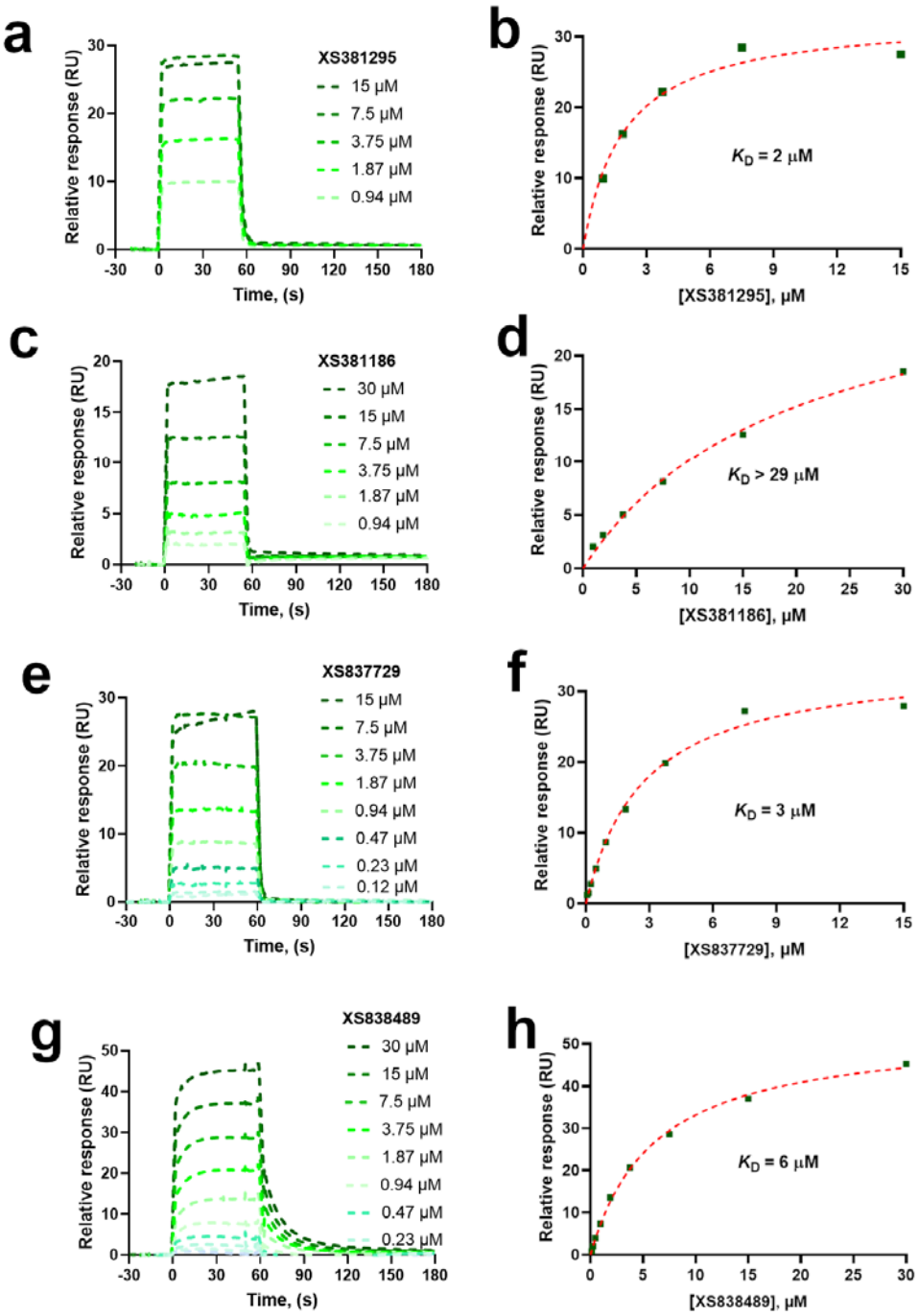

Supplementary Fig. 5 | Representative SPR sensorgrams (**a, c, e,** and **g**) and the response vs concentration plots (**b**, **d**, **f**, and **h**) for the four WDR91-specific EAS-MS hits: XS381295a (**a**, **b**), XS381186a (**c**, **d**), XS3837729 (**e**, **f**), and XS838489 (**g**, **h**). The response at equilibrium for each concentration were plotted against the compound concentration and affinity fitted by

applying 1:1 equilibrium binding model to extract the K_D of the interaction. The compounds were tested in duplicates. Data from one replicate is shown here for clarity.

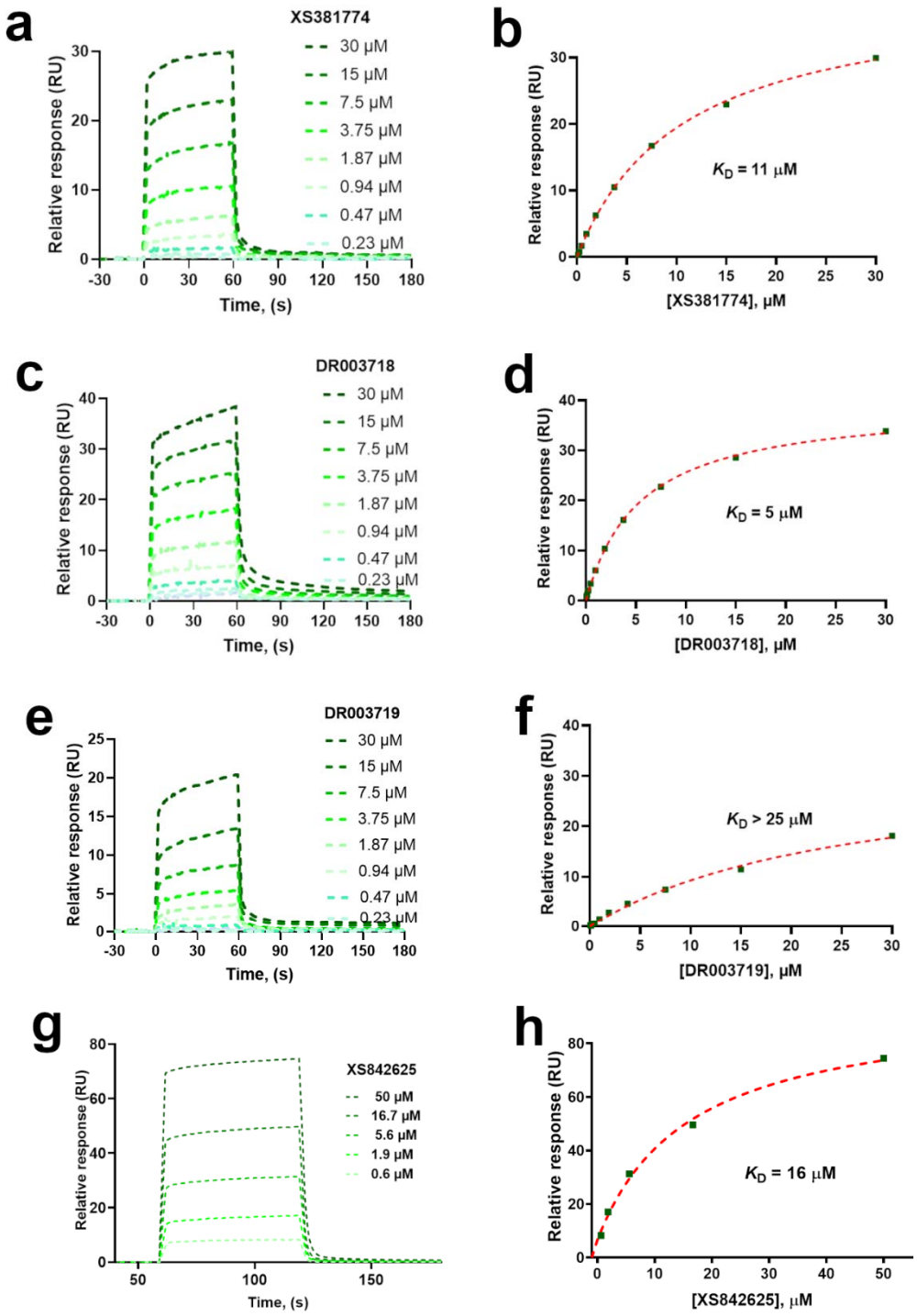

Supplementary Fig. 6 | Representative SPR sensorgrams (**a**, **c**, **e**, and **e**) and the response vs concentration plots (**b**, **d**, **f**, and **h**) for the WDR55 specific hit XS381774 (**a**, **b**) and its separated enantiomers DR003718 (**c**, **d**) and DR003719 (**e**, **f**), as well as XS842625 (**g**, **h**), respectively. The response at equilibrium for each concentration were plotted against the compound concentration and affinity fitted by applying 1:1 equilibrium binding model to calculate the K_D of the interaction. The compounds were tested in duplicates. Data from one replicate is shown here for clarity.

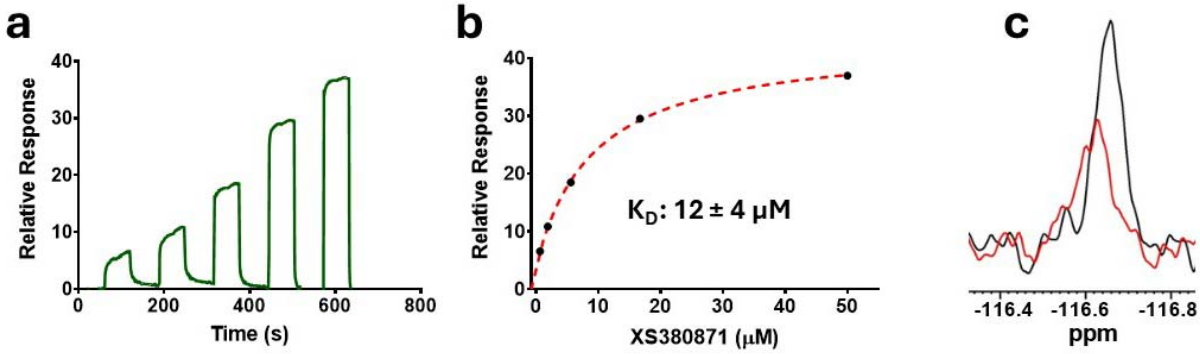

Supplementary Fig. 7 | Representative SPR sensorgram (**a**) and the steady-state response vs concentration plot (**b**) for the HAT1 specific hit XS380871. The response at equilibrium for each concentration were plotted against the compound concentration and affinity fitted by applying 1:1 equilibrium binding model (red dashed line), yielding a K_D value of 12 ± 4 μM. The experiments were performed in triplicate (n = 3). Data from one replicate is shown here for clarity. **(c)** Overlay of ^{19}F spectra of 20 μM XS380871 alone (black), and in the presence of ~34 μM of HAT1 (red).

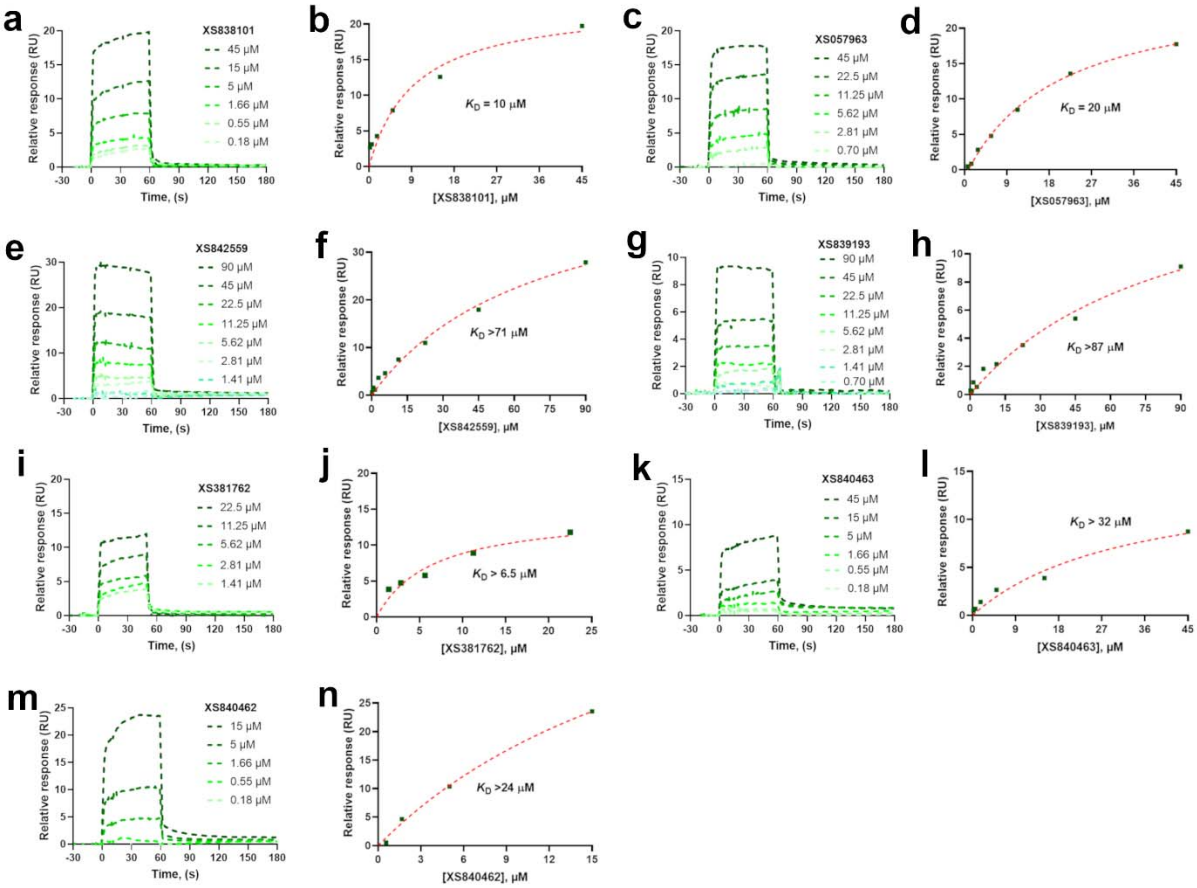

Supplementary Fig. 8 | Representative SPR sensorgrams (**a**, **c**, **e**, **g**, **i**, **k**, and **m**) and the response vs concentration plots (**b**, **d**, **f**, **h**, **j**, **l**, and **n**) for the SKP1 (**a**, **b**), DCAF1 (**c**, **d**), DCAF7 (**e**, **f**), FBXW7 (**g**, **h**), FBXO22 (**i**, **j**), AASS-LKR-GFP (**k**, **l**), and AASS-SDH-GFP (**m**, **n**) EAS-MS hits. The responses at equilibrium for each concentration were plotted against the compound concentration and affinity fitted by applying 1:1 equilibrium binding model to extract the K_D of the interaction. Where the K_D values are less/not reliable due to either sub stoichiometric binding or suboptimal concentration ranges for the dose-response titration were annotated by (>) sign. The compounds were tested in duplicates. Data from one replicate is shown here for clarity.

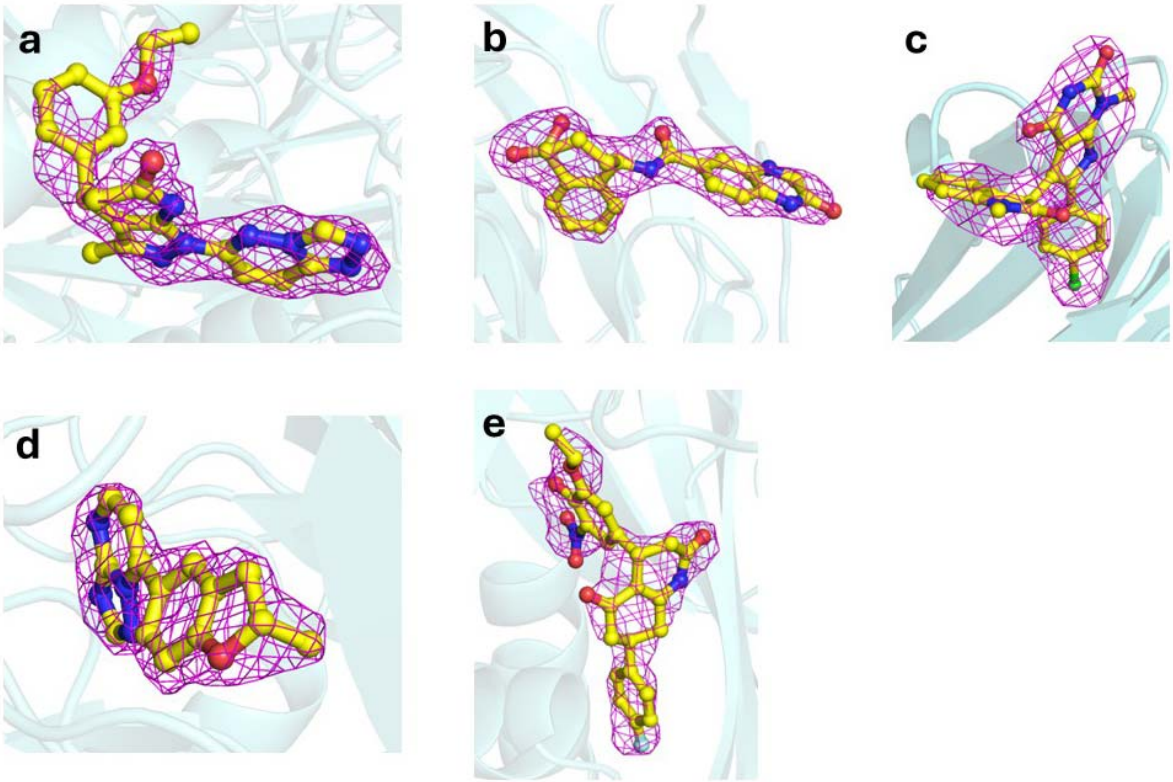

Supplementary Fig. 9 | The mFo-dFc electron density omit-maps for the EAS-MS hits (shown in yellow sticks) in the crystal structures of (**a**) DDB1_XS381952, (**b**) WDR91_XS838489, (**c**) WDR91_XS381295, (**d**) WDR55_XS381774, and (**e**) HAT1_XS380871 displayed as magenta meshes and contoured at 3σ.

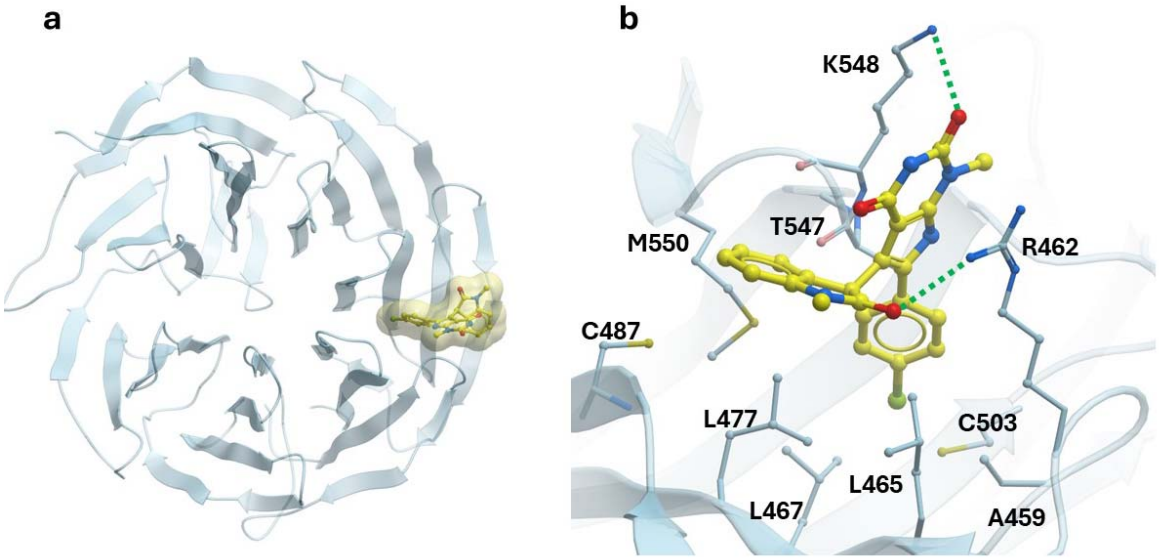

Supplementary Fig. 10 | Co-crystal structure of WDR91 in complex with XS381295. (**a**) Cartoon representation of WDR91 (cyan) bound to ligand (yellow). (**b**) Close-up view of the XS381295 binding site. Hydrogen bonds between the protein and the ligand are shown as black green dashed lines.

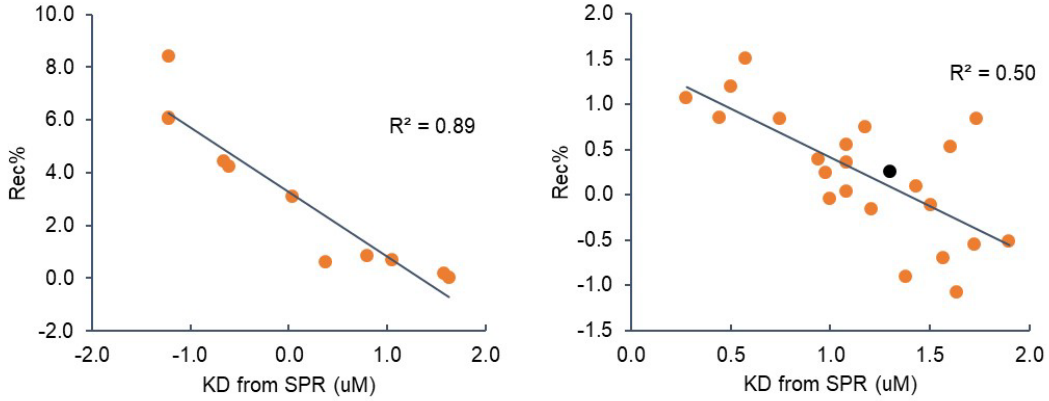

Supplementary Fig. 11 | Strong correlations between hit MS signals and K_D values of confirmed hits for single protein (WDR5, left) and all 11 proteins (right).

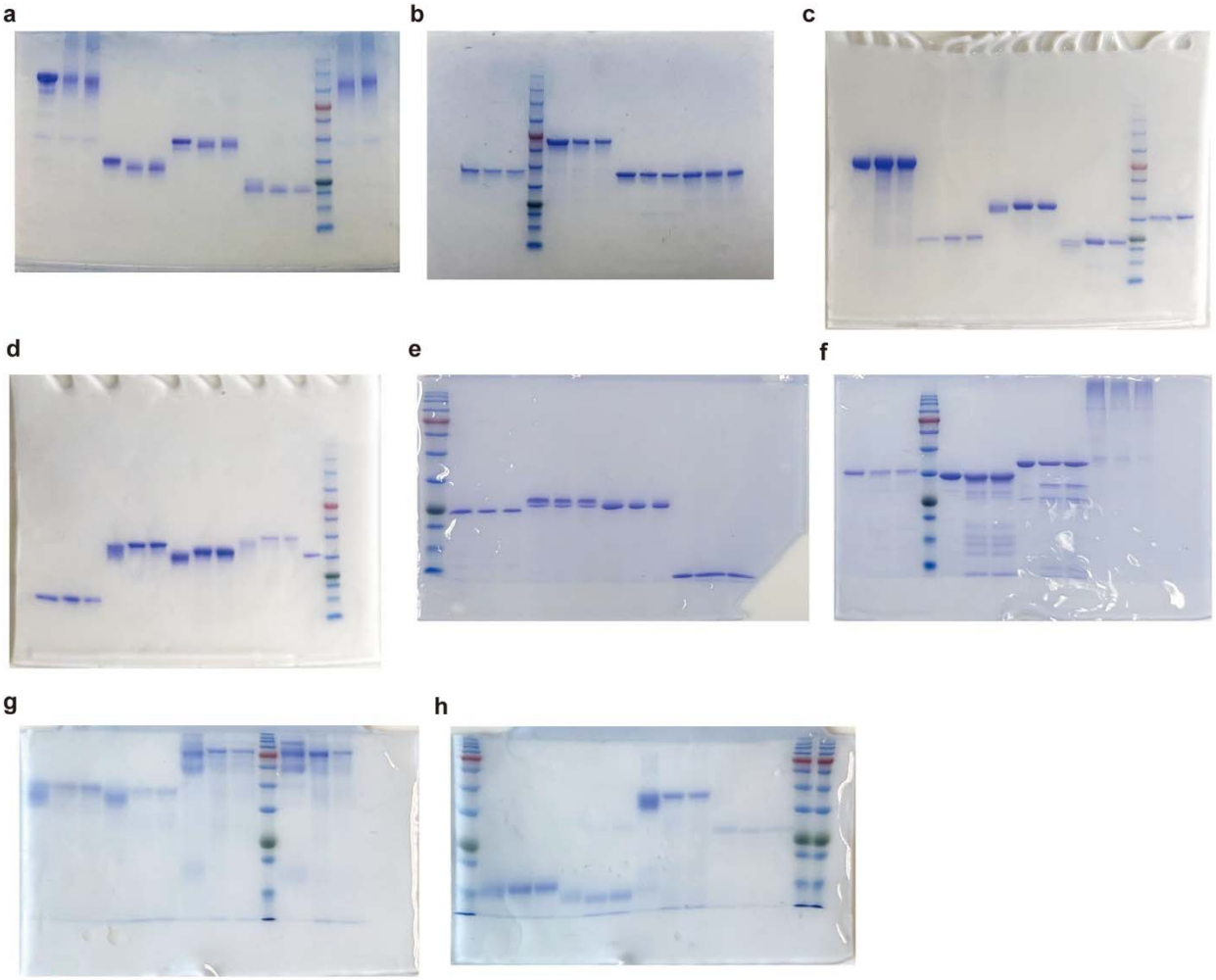

Supplementary Fig. 12 | Uncropped SDS-PAGE images. Each protein is shown in three lanes: total protein amount and two pulldown samples. (**a**) DDB1, COPB2(WDR), DCAF1(WDR), and DNMT3A. (**b**) LRRK2(WDR), NSP13, WDR91, and RFWD3. (**c**) DDX1, SETDB1, SEC31A, and SKP1. (**d**) MSH6, FBXW7, CHIP, and PIAS1. (**e**) TIF1A, TRIM28, SPSB2, and BIRC3(BIR1). (**f**) WDR55, TLE4, HAT1, and HTT. (**g**) THEMIS, DCAF7, AASS(LKR), and AASS(SDH). (**h**) YTHDC1, YTHDF2, and SKP1-FBXO22.

Supplementary Table 3. Data collection and refinement statistics

	WDR91_XS381295	WDR91_XS838489	DDB1_XS381952

PDB code	9EJO	9EJP	9EJQ
Data collection			
Space group	$C222_1$	$C222_1$	$P2_12_12_1$
Cell dimensions			
a, *b*, *c* (Å)	78.63, 132.38, 119.60	77.61, 132.55, 119.80	62.64, 124.70, 167.72
α, β, γ (°)	90.0, 90.0, 90.0	90.0, 90.0, 90.0	90.0, 90.0, 90.0
Resolution (Å)	50.0-2.40 (2.44-2.40)*	50.0-2.22 (2.26-2.22)*	50.0-1.87(1.90-1.87)*
R_{sym} or R_{merge}	0.086 (0.966)	0.062 (0.904)	0.068 (0.940)
CC1/2	0.999 (0.716)	1.001 (0.802)	0.999 (0.666)
I / σI	18.9 (1.9)	31.0 (2.7)	18.8 (1.9)
Completeness (%)	99.9 (100.0)	100.0 (100.0)	91.2 (94.1)
Redundancy	6.0 (6.0)	10.8 (10.8)	4.3 (4.7)
Refinement			
Resolution (Å)	27.70-2.40 (2.46-2.40)	44.67-2.22 (2.28-2.22)	25.10-1.87 (1.92-1.87)
No. reflections	23892	29329	94637
R_{work} / R_{free}(%)	19.9/23.8	20.3/24.5	16.4/22.0
No. atoms	2650	2682	9508
Protein	2535	2561	8739
Ligand/ion	30	27	29
Water	84	94	624
B-factors	48.0	48.5	31.5
Protein	48.1	48.5	30.8
Ligand/ion	55.5	57.6	45.2
Water	41.2	46.5	37.9
R.m.s. deviations			
Bond lengths (Å)	0.006	0.005	0.007
Bond angles (°)	1.295	1.342	1.282

*Values in parentheses are for highest-resolution shell.

Supplementary Table 3. Data collection and refinement statistics (continued)

	WDR55_XS381774	HAT1_XS380871
PDB code	9EKP	9MJG
Data collection		
Space group	$P2_1$	P1
Cell dimensions		
a, *b*, *c* (Å)	78.31, 58.41, 87.22	78.89, 87.84, 118.38
α, β, γ (°)	90.0, 96.3, 90.0	84.38, 80.07, 76.76
Resolution (Å)	34.81-1.95 (2.00-1.95)*	50.0-2.58 (2.62-2.58)*
R_{sym} or R_{merge}	0.082 (0.685)	0.127 (0.653)
CC1/2	0.998 (0.774)	0.984 (0.602)
I / σI	14.1 (2.4)	8.3 (1.3)
Completeness (%)	97.5 (95.9)	96.0 (76.5)
Redundancy	4.9 (5.0)	2.8 (2.3)
Refinement		
Resolution (Å)	34.83-1.95 (2.00-1.95)	49.45-2.58 (2.65-2.58)
No. reflections	53046	87207
R_{work} / R_{free}(%)	15.6/20.6	23.5/27.0
No. atoms	5101	20479
Protein	4696	20130
Ligand/ion	38	256
Water	339	93
B-factors	31.5	46.6
Protein	30.9	47.8
Ligand/ion	24.5	37.9
Water	39.4	26.0

R.m.s. deviations		
Bond lengths (Å)	0.005	0.005
Bond angles (°)	1.289	1.266

*Values in parentheses are for highest-resolution shell.

Supplementary Table 4. Detailed instrumental parameters of LC-MS.

Parameter setting of the mass spectrometer	
Ion Source:	
Spray Voltage: 3500 V (pos); 2500 V (neg)	Ion Transfer Tube Temperature: 325
Sheath Gas: 30 Arb	Auxiliary Gas: 10 Arb
Vaporize Temperature: 350	Ion Source Type: H-ESI
Full scan parameters:	
Scan range: 150-520 m/z	Resolution: 60,000
S-lens RF (%): 70	Automatic Gain Control (AGC) Target: Standard
DIA mode parameters for MS^2:	
Precursor Mass Range:	Resolution: 22,500
Isolation Window (m/z): 18	Window Overlap: 1 m/z
AGC Target: Standard	HCD Collision Energy (%): 15, 30, 60
Loop Control: N	N (Number of Spectra): 7